http://ansinet.com/itj

ITJ

ISSN 1812-5638

INFORMATION TECHNOLOGY JOURNAL

ANSInet
Asian Network for Scientific Information
308 Lasani Town, Sargodha Road, Faisalabad - Pakistan

Information Technology Journal 12 (7): 1289-1298, 2013
ISSN 1812-5638 / DOI: 10.3923/itj.2013.1289.1298

IHNS: A Pragmatic Investigation on Identifying Highly Noisy Subband in FMDFB for Fixing Threshold to Deteriorate Noise in Images

[1]S. Sutha, [2]E. Jebamalar Leavline and [3]D. Asir Antony Gnana Singh
[1]Department of Electrical and Electronics Engineering, University College of Engineering, Panruti, Anna University, Chennai, Tamilnadu, India
[2]Department of Electronics and Communication Engineering,
[3]Department of Computer Science and Engineering, Anna University Chennai, BIT Campus, Tiruchirappalli-620 024, Tamilnadu, India

Abstract: Multiscale image representation has been an area of interest in the recent past among the image processing society. Fast Multiscale Directional Filter Bank (FMDFB) is such a multiscale framework with interesting characteristics such as perfect reconstruction, directionality, less computational complexity and maximally decimated property. FMDFB is found suitable for a wide range of image processing applications like feature extraction and analysis. In this study, the application of FMDFB is extended to image denoising which is a vital pre-processing stage in almost all image processing and analysis systems. In this study, the statistical nature of the FMDFB subbands is analyzed. It is observed that, unlike wavelet subbands, each of the FMDFB subbands carries significant information about the image content. Hence, a mere wavelet based subband adaptive shrinkage method would oversmooth the FMDFB coefficients which in turn affects the quality of the denoised image. To overcome this, new method of selecting the suitable subband for estimating the threshold for noise removal is proposed. The threshold value for noise removal is estimated from the FMDFB subbands. For analysis purpose, the subband statistics of FMDFB is compared with the subband statistics of wavelet transform. The proposed NSS algorithm will be useful to calculate the suitable threshold value for image denoising with adaptive thresholding.

Key words: Image denoising, fast multiscale directional filter bank, noisy subband selection, threshold selection, wavelet transform, contourlet transform

INTRODUCTION

Image denoising has been a key area of interest in the past decade because of the growing information and communication technology. The sensor and circuitry of a scanner or digital camera in an image acquisition system causes random variations of brightness or colour information in images. Such random variations of brightness may also originate from film grain and the photon detector, which can be regarded as image noise (Stroebel and Zakia, 1995). The noisy components present in the digital images have to be removed (at least partially) before the image could be used for further analysis and processing. Noise removal is a process of estimating the clean image from its noisy observation. However, most of the noise removal methods require a prior knowledge about the noise distribution. This makes the noise removal process a challenging one (Gonzalez and Woods, 2002; Vaseghi, 2000).

Various types of noises such as Gaussian, Speckle and Salt and Pepper etc. are addressed in literature (Jain, 2003; Kaur *et al*., 2003) according to the probability distribution of the noise function. Starting from the well-known spatial filtering methods, a number of denoising algorithms have been proposed in the literature for removing various types of noises. The purpose of filtering is to cancel out noisy picture elements while preserving the integrity of edge and detail information. Conventional linear filters such as arithmetic mean filter and gaussian filter smoothes noises efficiently, yet they blur edges because of local averaging operators. Nonlinear filtering techniques remove noisy components and preserve edges better than linear filtering (Gonzalez and Woods, 2002). The Wiener filtering is one such method that is mean square error-optimal stationary linear filter for images degraded by additive noise and blur (Vaseghi, 2000). However, a common drawback of the practical use of this method is that they usually require

Corresponding Author: E. Jebamalar Leavline, Department of Electronics and Communication Engineering, Anna University Chennai, BIT Campus, Tiruchirappalli- 620 024, Tamilnadu, India

some 'apriori' knowledge about the spectra of noise and the original signal. This information is needed to perform the optimal choice of parameter values and/or threshold selections (Kaur *et al*., 2003; Bamberger and Smith, 1992). Unfortunately, such information is very often not available when real time images are handled. This makes the spatial techniques less effective for noise removal in various applications.

Alternatively, denoising methods using various transforms have been proposed. Wavelet transform has proved itself best suited for several image processing applications including denoising (Boggess and Narcowich, 2002; Soman and Ramachandran, 2005) over Discrete Cosine Transform (DCT) and Fast Fourier Transform (FFT) approaches. Also there are well known shrinkage methods for wavelet based denoising (Soman and Ramachandran, 2005; Leavline *et al*., 2011). Unfortunately, the denoised images resulting from the wavelet-based denoising have checkerboard artifacts. Natural images contain discontinuity points (e.g.: Edges) located along smooth curves (i.e., Contours). Separable wavelets can capture only limited directional information because of the poor directional selectivity of wavelet transform. These behaviors indicate that representations that are more powerful are needed in higher dimensions with directional selectivity. Also, for the human visual system, the receptive fields in the visual cortex are characterized as being localized, oriented and bandpass and tuned to capture the essential information of the natural scene using a least number of visually active cells (Do and Vetterli, 2005). This leads to development of representations which are sparse, local, directional and multiresolution.

There are number of such representations introduced in the literature namely Gabor wavelets (Lee, 1996), Brushlets (Meyer and Coifman, 1997), Bandlet (Pennec and Mallat, 2005), Curvelet (Candes and Donoho, 1999) (Do and Vetterli, 2001), Shearlet (Guo and Labate, 2007), Directionlets (Velisavljevic *et al*., 2006) and Contourlet (Do and Vetterli, 2005) etc. with their own pros and cons. Contourlet may be regarded as a transform which exhibits interesting properties such as Multiresolution, Localization, Critical sampling, Directionality and Anisotropy which are much important in representing local geometrical features. Further, Contourlet representation of an image is overcomplete with a redundancy ratio of 4/3 (Do, 2001). The Multiscale Directional Filter Banks (MDFB) proposed by Kin-On Cheng *et al*. (2007a) modifies the Pyramidal Directional Filter Bank (PDFB) or the Contourlet transform by splitting the finest frequency scale in LP into two frequency bands. MDFB improves the radial frequency resolution of the Contourlet transform by introducing an additional decomposition in the high-frequency band. Further, directional decompositions are performed prior to scale decomposition. Since no decimation is introduced in the new scales, MDFB possess higher redundancy than the Contourlet Transform (Cheng *et al*., 2007a).

Faster version of this MDFB was proposed by Cheng *et al*. (2007b) namely Fast Multiscale Directional Filter Banks (FMDFB) by swapping scale and directional decomposition in the first two scales. According to Cheng *et al*. (2007b) this fast structure has reduced computational complexity and well suited for representing images in various applications. In our previous study, the application of FMDFB was extended to image denoising with global thresholding approach, which outperformed conventional contourlet based denoising. Further, in this study, we analyze the statistical nature of the FMDFB subbands and it is compared with that of the wavelet transform to show the significant characteristics of the FMDFB subbands. In order to determine the threshold from the subband statistics, a new approach namely noisy subband selection algorithm is proposed. Using NSS algorithm, the subband with huge amount of noisy components is identified at each stage of FMDFB decomposition thus the threshold can be made adaptive for better denoising performance.

MATERIALS AND METHODS

Multiscale image representations: Multiscale transforms represent an image in different scales thereby ensuring the frequency resolution of the content of interest. In addition, they possess the most advantageous features such as sparsity and hence acquire high degree of energy compaction, that is useful in compression applications. The well-known multiscale transform namely Contourlet transform finds applications in various fields of image processing. Unlike separable wavelet transform, these Contourlet bases exhibits some interesting characteristics like Multiresolution, localization, critical sampling, directionality and anisotropy (Cheng *et al*., 2007a). Among these, the first three are successfully given by separable wavelets; Contourlet that can retain significant directional information supports the latter two. In Contourlet transform, the sparse representation is obtained by first applying a multiscale transform followed by a local directional transform to capture local features such as edges.

Multiscale directional filter banks (MDFB): The MDFB alter the pyramidal directional filter bank or Contourlet Transform by introducing scale decomposition in its finest scale. Scale decomposition is done by performing low pass filtering with cut-off frequency 0.75 ∏ to an input image (Cheng *et al*., 2007b). First scale is generated by subtracting the lowpass image from the input image. Second scale is obtained as the first band pass image in LP. Third scale is the second band pass image in LP and so on. It contains two basic building blocks namely Laplacian Pyramid (LP) and Directional Filter Bank (DFB).

Laplacian pyramid: An efficient way of obtaining multiscale decomposition is to use a low pass filter (Burt and Adelson, 1983) called Laplacian Pyramid. It is an over complete decomposition in which input image is represented by a set of band pass images and a low pass image. In the LP, a lowpass filter and a downsampler first process the input image to generate a lowpass image. A coarse prediction of the original image is computed by upsampling and subsequently convolving the lowpass image using another lowpass filter. By subtracting the coarse prediction from the input signal, a bandpass image is obtained. The process can be iterated on the lowpass image to generate other bandpass images in lower frequency range. A drawback of LP is the implicit oversampling. A block diagram of this iterative process is shown in Fig. 1. The main feature of the LP is that decimation is performed only on the lowpass image. Thus, there is no frequency scrambling.

To avoid aliasing in the LP, it requires the stopband edge of $h_L(n)$ should be less than ∏/2. In order to satisfy the criteria, equiripple hL(n) with pass band edge 0.3 ∏ and stop band edge 0.5 ∏ are designed (Cheng *et al*., 2007b; Do and Vetterli, 2003). Further, processing such as directional decomposition can be performed directly on the bandpass images.

Directional filter bank: Directional filter bank (DFB) introduced in 1992 (Bamberger and Smith, 1992). It is a 2-D directional filter bank is a critically sampled directional decomposition with perfect reconstruction property. The DFB partitions a frequency plane into a set of wedge-shape region as illustrated in Fig. 2.

It can be implemented efficiently in an 'l' level tree structure that results in 2' directional subbands. The tree structure relies on a two-channel filter bank in which a complementary diamond-shaped filter pair is followed by a quincunx down sampling as shown in Fig. 3 (Do, 2001; Cheng *et al*., 2007a).

A resampler is employed before the two-channel filter bank. Its function is to shear the desired frequency

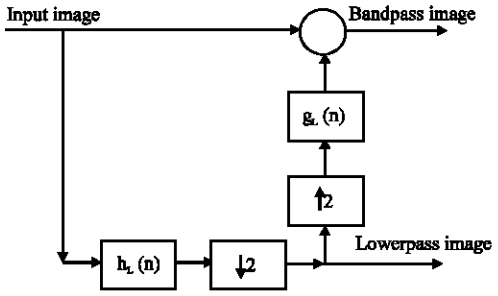

Fig. 1: Iterative structure of the laplacian pyramid, $h_L(n)$ is the lowpass filter, $g_L(n)$ is the high pass filter, ↑2 and ↓2 represents down sampling and upsampling by a factor of 2, respectively

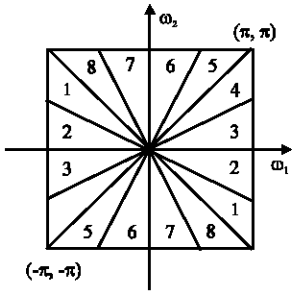

Fig. 2: Frequency plane partitioning in a three-level DFB

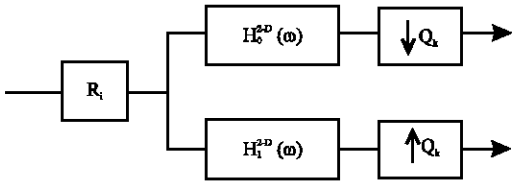

Fig. 3: Two channel DFB (Ri-Resampling Matrix, H_0, H_1: Low pass filters, Q_k: Quincunx down sampling)

partitions into diamond shape so that the two-channel filter bank can give the desired frequency bands.

Resampling: The definition of resampling matrix is that it is a 2×2 matrix whose entries are all integers and whose determinant is non zero so that its inverse matrix is also a resampling matrix. It is a unimodular matrix that can change the diamond shaped pass band into parallelogram pass band. A unimodular matrix is a matrix whose determinant is ±1. Its inverse is also unimodular. There are many resampling matrices have been proposed in the literature (Bamberger and Smith, 1992; Do, 2001). Any one of the following can be used according to the required frequency band:

$$R_1 = \begin{pmatrix} 1 & 1 \\ 0 & 1 \end{pmatrix} \quad R_2 = \begin{pmatrix} 1 & -1 \\ 0 & 1 \end{pmatrix}$$
$$R_3 = \begin{pmatrix} 1 & 0 \\ 1 & 1 \end{pmatrix} \quad R_1 = \begin{pmatrix} 1 & 0 \\ -1 & 1 \end{pmatrix} \tag{1}$$

Figure 4 shows, for R_1 and R_2, the input image is extended along the vertical direction; while for R_3 and R_4 the image is extended along the horizontal direction.

Diamond shaped filters: Diamond shaped filter pair splits the frequency spectrum of the input signal into lowpass and highpass channels (Bamberger and Smith,1992). Figure 5 shows the frequency spectrum of diamond shaped filter.

One filter pair can be derived from the other by simply modulating the filters by $\prod$ in either the ω_1 or ω_2 frequency variable. Perfect reconstruction is achieved by applying the same modulation to both analysis and synthesis filters. Because of sampling, subbands would suffer from spatial distortion. Spatial distortion results from resampling used in the construction. This problem can be solved by adopting backsampling at the output of the DFB (Do, 2001). The overall sampling matrix is given by:

$$s = \begin{cases} D_0^{i-2} \text{ in } R_0 \\ D_0^{i-2} \text{ in } R_1 \end{cases} \tag{2}$$

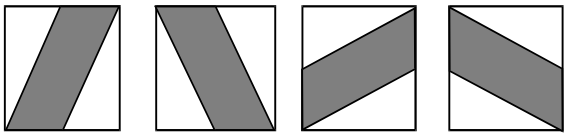

Fig. 4: Four parallelogram pass bands produced by R_1, R_2, R_3 and R_4, respectively

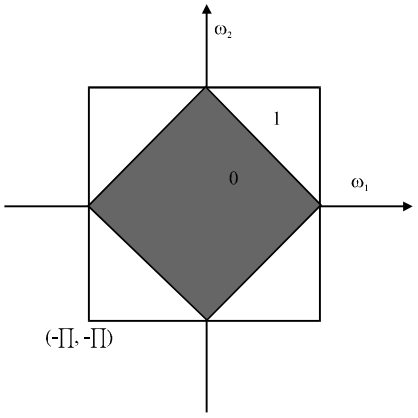

Fig. 5: Frequency spectrum of diamond shaped filter (Stopband is shown in gray)

where, 'i' is the index of output stage of DFB, R_j, j = 0, 1 are the spectral regions shown in Fig. 6, D_0 and D_1 are Downsampling matrices:

$$D_0 = \begin{pmatrix} 2 & 0 \\ 0 & 1 \end{pmatrix} \quad D_1 = \begin{pmatrix} 1 & 0 \\ 0 & 2 \end{pmatrix} \tag{3}$$

The backsampling reorders the subbands so that the overall sampling is diagonal (Cheng *et al*., 2007b).

Quincunx down sampling: It is a generalized down sampling matrix is a sampling matrix whose entries are ±1 with determinant 2. The resampling matrices are used to perform the shearing operation (Do, 2001). The quincunx matrices that can be used in directional filter banks are derived as follows:

$$Q_1 = R_2 D_0 R_3 = R_3 D_1 R_2$$
$$Q_2 = R_1 D_0 R_4 = R_4 D_1 R_1 \tag{4}$$

Out of the above four quincunx sampling matrices any one can be used for down sampling. Those sampling matrices generate the same sub-lattice but the down sampling operation rotates the input image by -45 and 45°. Quincunx down sampling results in down sampled and rotated representations as shown in Fig. 7.

Fast multiscale directional filter banks (FMDFB): The basic building blocks of Fast Multiscale Directional Filter banks are the same as that of MDFB namely, Laplacian Pyramid and Directional Filter Banks (Cheng *et al*., 2007b). In analysis filter bank structure, low pass filtering and wavelet transform technique are applied for splitting the image into various scales. Use of non aliasing lowpass filters broadens the bandwidth of the finer scale.

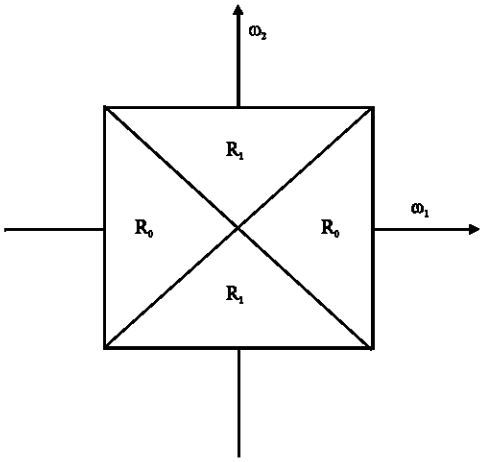

Fig. 6: Spectral regions R_0 and R_1

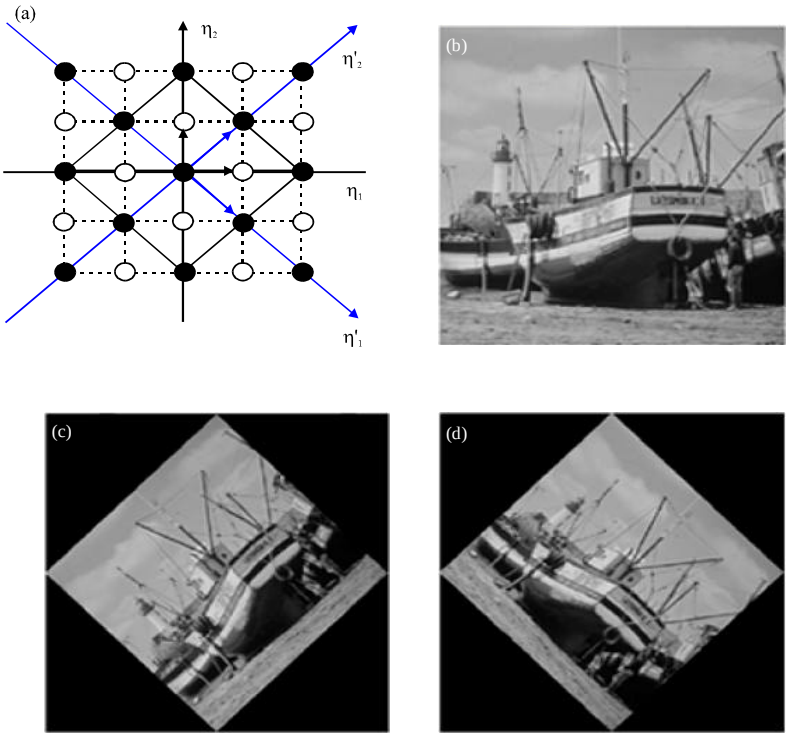

Fig. 7(a-d): (a) Example of quincunx downsampling lattice in (n_1,n_2) space, (b) An input image, (c) and (d) Quincunx downsampled outputs by q_1 and q_2, respectively

Directional decomposition with lower angular resolution is performed before scale decomposition. Hence, one set of operations for directional decomposition with lower angular resolution is saved by sharing. Also, the total number of subband coefficients will be equal to the size of the original image and thereby maintaining the maximally decimated property. As stated in (Cheng *et al*., 2007b), perfect reconstruction is always possible at all scales regardless of the low pass filters used for decomposition. According to Cheng *et al*. (2007b) this FMDFB achieved 33.5-37.5% of reduction in computational complexity when compared to original MDFB.

Denoising using FMDFB: David L. Donoho proposed a method for reconstructing an unknown function 'f' on (0, 1), from noisy data (Boggess and Narcowich, 2002) with wavelet thresholding. The reconstruction is defined in wavelet domain as translation of all the empirical wavelet coefficients toward zero by an amount of threshold 'T'. Further, adaptive threshold estimation methods have been used for wavelet domain image denoising (Suresh *et al*., 2007) and proved computationally more efficient and adaptive since the parameters required for estimating the threshold depend only on the subband data. Adaptive thresholding methods are also found to study well with Contourlet (Zhou and Shui, 2007).The adaptive window in each of the Contourlet subband is first fixed by autocorrelation function of Contourlet coefficients' energy distribution, followed by the local Wiener filtering to denoise the noisy image.

In general, there are three steps in transform domain denoising:

- Transform the input data by an orthogonal transform
- Threshold transformed coefficients by a nonlinear algorithm
- Reconstruct image with modified coefficients

Wavelet shrinkage is an efficient signal denoising algorithm introduced by Donoho (1993) which is based on the idea that the original image has large wavelet coefficients and the noise is distributed over all coefficients. Thus, by thresholding (either hard threshold or soft threshold) (Wang and Zheng, 2013) the smaller coefficients, the image will not be damaged, even though a large amount of noise energy will be removed Hard threshold follows 'Keep or kill' approach which exhibits

some oscillations near edges. On the other hand in Soft threshold small coefficients are cancelled and the others are changed in order not to destroy the continuity in transformed coefficients (Donoho, 1993).

In our previous study the fast multiscale filter banks is used to obtain the transformed coefficients (Leavline and Sutha, 2011). The algorithm for image denoising using FMDFB is described below:

- Get the input image
- Decompose the noisy image with FMDFB. The FMDFB analysis filter bank decomposes the input noisy image in to '2' subbands for the decomposition level of 'l'
- Estimate Median Absolutes Difference (MAD) and noise variance
- Determine threshold value with the parameters calculated in step 3. The value of threshold depends on the choice of thresholding method
- Perform soft thresholding with global threshold approach
- Apply inverse FMDFB to the threshold coefficients and reconstruct the image
- Obtain the denoised image and calculate Peak Signal to Noise Ratio using the formula:

$$\text{PSNR} = 10\log_{10}\left(\frac{255^2}{\text{MSE}}\right) \quad (5)$$

The process flow of the denoising algorithm is shown in Fig. 8.

Noisy subband selection in FMDFB: In our previous study Wavelet based shrinkage functions with global threshold approach were employed (Leavline and Sutha, 2011) which outperformed the conventional contourlet based denoising algorithm in terms of PSNR. In wavelet decomposition, out of four subbands at any level of decomposition, the approximate coefficients contain the coarse information of the image and the high frequency fine details are present in the other three subbands

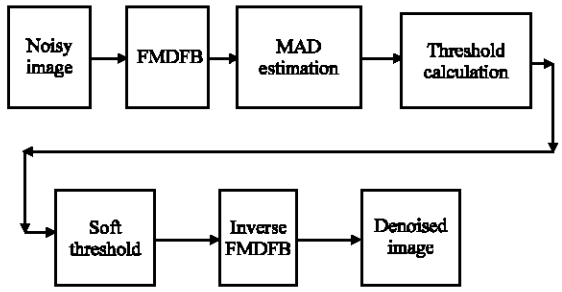

Fig. 8: Denoising scheme using FMDFB

namely Horizontal, Vertical and Diagonal subbands (Soman and Ramachandran, 2005; Zhou and Shui, 2007). On the other hand, the FMDFB subbands carry image information is in almost all subbands at any level (l) of decomposition. Also, in contrary with wavelet decomposition, the number of subbands of FMDFB depends on the number of levels of DFB (Cheng *et al*., 2007b). For two levels of decomposition, wavelets produce seven subbands (A_2, V_2, H_2, D_2, V_1, H_1 and D_1) where with the number of DFB levels l = 2, at scale S_i = 2, FMDFB yields 16 ($2^l \times 2^S$) subbands. Hence, a mere global threshold is less effective in noise removal with FMDFB.

To achieve better denoising performance, it is apparent that, the selection of suitable threshold is vital. In this direction, a nonlinear function, which considerably shrinks the noisy coefficients, retaining the image details has to be developed. For real time image processing applications, particularly when the noise power is unknown, it has to be estimated without the prior knowledge of noise distribution. In the next section we propose a new scheme to identify the noisiest subband out of 2×2^S FMDFB subbands and to estimate the noise power from the statistics of the subbands.

Proposed NSS (noisy subband selection) algorithm: The proposed NSS algorithm works as follows. The noisy image is first decomposed to 2' subbands at stage 1 each of size N/2×N/2 for a N×N image. For each subband, standard deviation is calculated and the subband with maximum standard deviation is considered as noisy subband. Then, the threshold for stage-1 is calculated with the maximum standard deviation and applied to all coefficients in stage-1 using soft threshold technique. Similarly higher stages of decomposition are performed, at each stage the standard deviation of the noisiest subband and the threshold value are calculated and applied on the coefficients. This process is repeated until the subband size is negligibly small.

Parameters:

l = No. of levels in DFB
S = No. of scales in FMDFB
S_i = Scale index

Algorithm:

Step 1: Get the noisy image
Step 2: Determine the number of levels in DFB (l) and FMDFB (S)
Step 3: Decompose the noisy image into subbands ($2^l \times 2^S$)
Step 4: Obtain the subband coefficients at the first stage of decomposition
Step 5: Calculate standard deviation of each subband
Step 6: Identify the subband with maximum standard deviation and designate the corresponding subband as Noisy subband at that level
Step 7: Estimate threshold for stage-1, using the maximum standard deviation and apply to all subbands in stage-1
Step 8: Repeat step 5-7 for next higher stage of decomposition

With this NSS algorithm, the noise standard deviation is estimated from the FMDFB subband statistics which is used to calculate the threshold value for denoising. Calculation of threshold for each stage and denoising is beyond the scope of this study. However, the threshold methods such as Vishushrink, SUREshrink, Normalshrink and Bayes shrink (Leavline *et al*., 2011; Wang and Zheng, 2013) can be used to calculating the threshold. After applying adaptive threshold, inverse FMDFB can be applied to reconstruct the denoised image.

RESULTS AND DISCUSSION

The experiments have been carried out with MATLAB 7.5.0 (R2007b) on a set of standard Gray scale images of size 512×512. In FMDFB, the number of DFB levels is set as 2 and two stages of scale decomposition have been performed. After decomposition, the NSS algorithm is applied on the 16 ($2^l \times 2^s$) decomposed subbands to find out the noisy subband. This algorithm is also employed on wavelet subbands for its sound justification. The comparison of standard deviation of Wavelet subbands for standard test images (Peppers, Mandrill and Barbara) are shown in Fig. 9 and 10 with one level and two levels of decomposition respectively. It is evident from Table 1 that the minimum subband standard deviation always occurs at HH1 subband of the wavelet decomposition. Also the maximum standard deviation is exhibited by the approximate (LL) coefficients of the finest level.

The graphical representation of Standard deviation of all '2l' FMDFB subbands (l = 2) with one level decomposition (SB1, SB2, SB3 and SB4) for Peppers, Mandrill and Barbara images are shown in Fig. 11. Figure 12(a-c) shows standard deviation of all '$2^l \times 2^s$' FMDFB subbands (l = 2, s = 2) with two levels of decomposition (SB1q, SB2q, SB3q and SB4q) for Peppers, Mandrill and Barbara images respectively. From Fig. 11 it is observed that the maximum subband standard deviation occurs in any one of the four subbands at level 1. Table 2 also appreciates this fact. From the experimental results tabulated in Table 2 and 3 the following facts are observed. In contrary with the wavelet decomposition at level 1, the noise spread is wider and the higher subband standard deviation lies on any one of the FMDFB subbands (SB_1, SB_2, SB_3 and SB_4). For smooth images, the subband standard deviations are found to be lower compared to that of images with more details. In level 2,

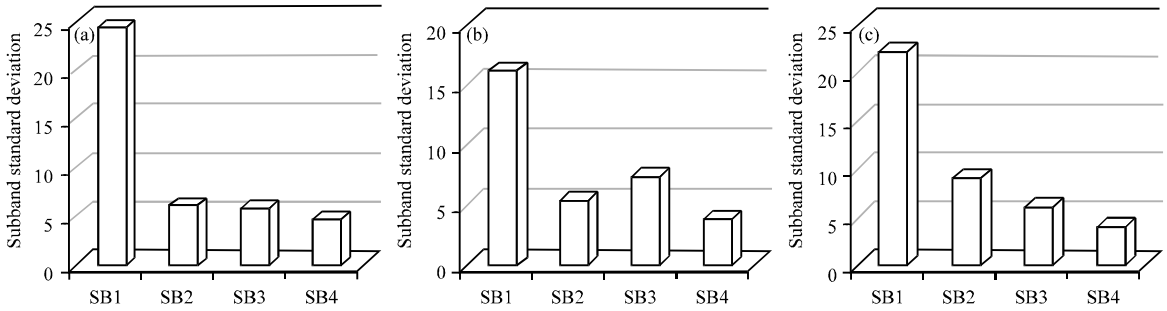

Fig. 9(a-c): Standard deviation of Wavelet subbands with one level decomposition for Peppers, Mandrill and Barbara images, respectively

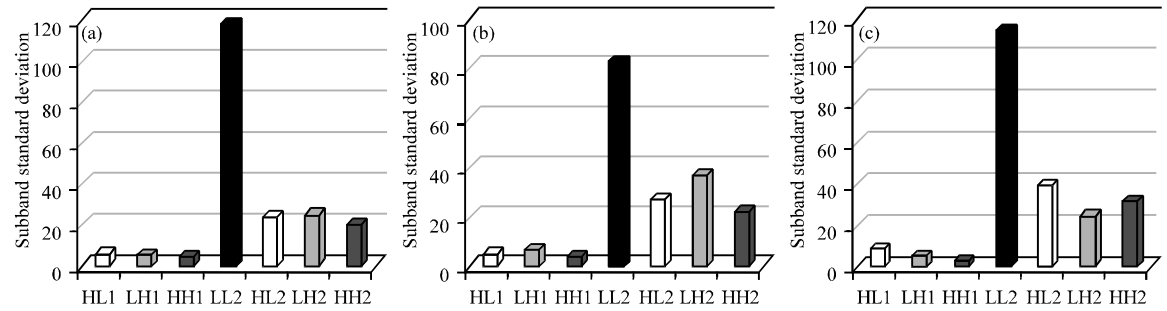

Fig 10(a-c): Standard deviation of Wavelet subbands with two levels of decomposition for Peppers, Mandrill and Barbara images, respectively

Table 1: Standard deviation of Wavelet subbands with two levels of decomposition for various images

	Subband standard deviation							
Test image	LL1	HL1	LH1	HH1	LL2	HL2	LH2	HH2
Peppers	24.424	6.154	5.919	4.734	118.599	24.291	25.476	20.867
Barbara	22.172	9.181	6.152	4.018	114.590	39.877	25.607	32.403
Boat	21.089	5.536	5.510	3.577	105.794	25.142	23.100	19.423
Goldhill	11.032	6.030	5.760	3.894	54.319	24.487	24.037	19.457
Lena	29.074	5.067	4.549	3.725	148.068	27.744	21.690	19.269
Mandrill	16.179	5.476	7.361	3.872	82.753	27.464	37.203	22.417
Zelda	19.287	5.272	5.795	4.042	100.682	24.658	22.656	19.289
Aerial	14.273	4.635	4.985	3.581	74.596	25.235	27.324	19.683
Airfield	27.073	6.193	5.784	4.263	122.805	33.447	35.253	21.484
Bridge	19.986	4.770	5.256	3.566	100.657	25.034	23.988	20.735

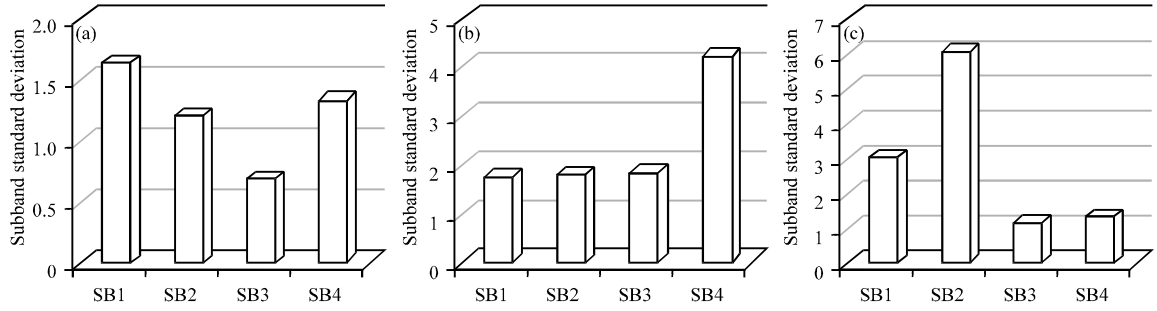

Fig 11(a-c): Standard deviation of all '2' FMDFB subbands (l = 2) with one level decomposition (SB1, SB2, SB3 and SB4) for Peppers, Mandrill and Barbara images, respectively

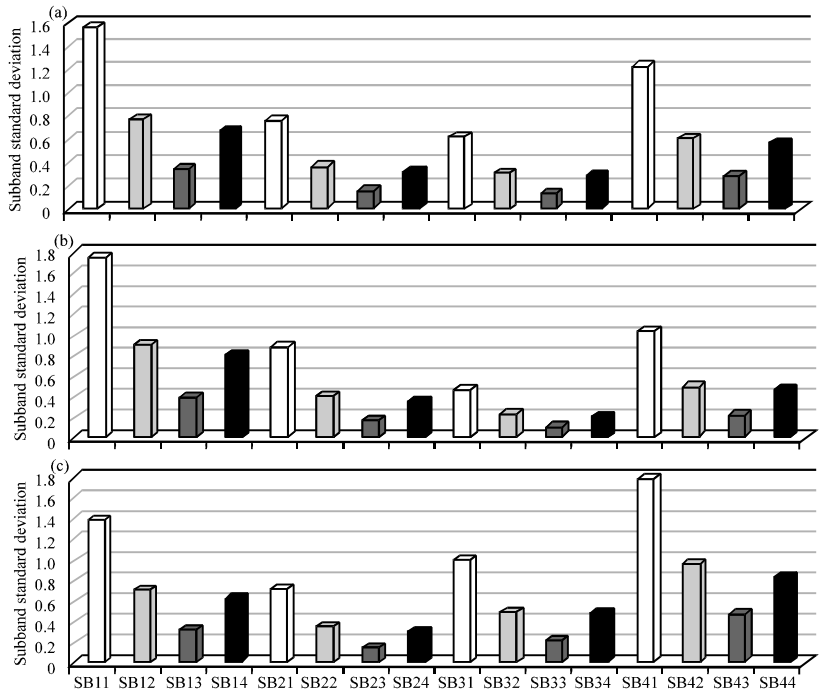

Fig. 12(a-c): FMDFB standard deviation of all '2'×2^s' subbands (l = 2, s = 2) with two levels of decomposition (SB1q, SB2q, SB3q and SB4q) for Peppers, Mandrill and Barbara images, respectively

unlike level 1, for all test images, higher subband standard deviation lies on SB_{11}, SB_{21}, SB_{31} and SB_{41} which are derived after second scale decomposition of SB_1, SB_2, SB_3 and SB_4, respectively. Another significant inference is

Table 2: Standard deviation of FMDFB subbands with one level decomposition for various images

	Subband standard deviation			
Test image	SB1	SB2	SB3	SB4
Barbara	3.049	6.065	1.197	1.339
Boat	1.440	1.563	0.660	1.241
Goldhill	1.396	1.262	0.613	1.332
Lena	1.293	1.237	0.579	1.236
Mandrill	1.777	1.835	1.858	4.247
Peppers	1.648	1.219	0.703	1.341
Zelda	1.325	1.099	0.658	1.132
Aerial	1.421	1.276	0.765	1.652
Airfield	1.710	2.025	0.950	2.142
Bridge	1.753	1.650	0.942	1.841

Table 3: Standard deviation of FMDFB subbands with two levels of decomposition for various images

	Subband standard deviation															
Test image	SB11	SB12	SB13	SB14	SB21	SB22	SB23	SB24	SB31	SB32	SB33	SB34	SB41	SB42	SB43	SB44
Barbara	1.77	0.91	0.41	0.81	0.89	0.42	0.18	0.37	0.48	0.24	0.11	0.22	1.05	0.50	0.23	0.48
Boat	1.23	0.61	0.27	0.53	0.61	0.34	0.15	0.28	0.50	0.26	0.11	0.23	1.01	0.48	0.22	0.44
Goldhill	1.42	0.67	0.31	0.66	0.86	0.47	0.20	0.37	0.57	0.28	0.12	0.24	1.10	0.59	0.26	0.49
Lena	1.15	0.56	0.25	0.51	0.76	0.37	0.17	0.34	0.50	0.24	0.11	0.23	0.99	0.47	0.21	0.45
Mandrill	1.40	0.72	0.33	0.63	0.73	0.36	0.16	0.31	1.01	0.50	0.24	0.50	1.80	0.97	0.49	0.85
Peppers	1.59	0.79	0.36	0.69	0.78	0.39	0.18	0.34	0.63	0.32	0.15	0.30	1.24	0.62	0.30	0.58
Zelda	1.30	0.66	0.31	0.60	0.71	0.36	0.16	0.31	0.58	0.29	0.14	0.27	0.96	0.52	0.23	0.43
Aerial	1.38	0.69	0.34	0.66	0.62	0.34	0.15	0.28	0.62	0.29	0.14	0.30	1.14	0.55	0.27	0.55
Airfield	1.38	0.72	0.34	0.64	0.81	0.45	0.20	0.37	0.53	0.25	0.12	0.25	1.07	0.54	0.25	0.49
Bridge	1.39	0.69	0.33	0.64	0.68	0.39	0.17	0.32	0.62	0.32	0.16	0.31	1.25	0.61	0.31	0.61

that at level 2 there is a higher degree of regularity i.e., for all test images higher subband standard deviation is observed at SB_{11}, SB_{21}, SB_{31} and SB_{41}.

In summary, the maximum or minimum standard deviation in FMDFB subbands occurs in any one of the '2'×2" subbands. Hence, a mere wavelet-like subband selection for estimating threshold is not sufficient for FMDFB based noise removal.

CONCLUSION

In this study, the statistical nature of the FMDFB subbands are analysed and the NSS algorithm is proposed to select the suitable FMDFB subband to estimate threshold for noise removal. This algorithm was employed on both Wavelet and FMDFB subbands for its sound analysis and justification with a huge set of standard test images. The experimental analyses show that, maximum or minimum standard deviation in FMDFB subbands occurs in any one of the '2'×2" subbands which is not so in case of wavelet subbands. Hence, a mere wavelet-like subband selection for estimating threshold is not sufficient for FMDFB based image noise removal. The proposed NSS algorithm will be useful to calculate the suitable threshold value at each decomposition stage for image denoising with adaptive thresholding.

REFERENCES

Bamberger, R.H. and M.J.T. Smith, 1992. A filter bank for the directional decomposition of images: Theory and design. IEEE Trans. Signal Process., 40: 882-893.

Boggess, A. and F.J. Narcowich, 2002. A First Course in Wavelets with Fourier Analysis. Prentice Hall, Upper Saddle River, NJ.

Burt, P.J. and E.H. Adelson, 1983. The laplacian pyramid as a compact image code. IEEE Trans. Commun., 31: 532-540.

Candes, E. and D. Donoho, 1999. Curvelets: A Surprisingly Effective Nonadaptive Representation of Objects with Edges. In: Curves and Surfaces, Schumaker, L. L. *et al*. (Eds.). Vanderbilt University Press, Nashville, TN.

Cheng, K.O., N.F. Law and W.C. Siu, 2007a. Multiscale directional filter bank with applications to structured and random texture retrieval. Pattern Recognit., 40: 1182-1194.

Cheng, K.O.O., N.F.F. Law and W.C.C. Siu, 2007b. A novel fast and reduced redundancy structure for multiscale directional filter banks. IEEE Trans. Image Process., 16: 2058-2068.

Do, M.N. and M. Vetterli, 2001. Pyramidal directional filter banks and curvelets. Proceedings of the IEEE International Conference Image Processing, October 7-10, 2001, Thessaloniki, Greece, pp: 158-161.

Do, M.N. and M. Vetterli, 2003. Framing pyramids. IEEE Trans. Signal Process., 51: 2329-2342.

Do, M.N. and M. Vetterli, 2005. The contourlet transform: An efficient directional multiresolution image representation. IEEE Trans. Image Process., 14: 2091-2106.

Do, M.N., 2001. Directional multiresolution image representations. Ph.D. Thesis, Department of Communication Systems, Swiss Federal Institute of Technology Lausanne.

Donoho, D.L., 1993. De-noising by soft thresholding. IEEE Trans. Inf. Theory, 43: 933-936.

Gonzalez, R.C. and R.E. Woods, 2002. Digital Image Processing. 2nd Edn., Prentice Hall, New Jersey, USA., ISBN-10: 0201180758.

Guo, K. and D. Labate, 2007. Optimally sparse multidimensional representation using shearlets. SIAM J. Math. Anal., 39: 298-318.

Jain, A.K., 2003. Fundamentals of Digital Image Processing. Prentice Hall, Englewood Cliffs, New Jersey.

Kaur, L., S. Gupta and R.C. Chauhan, 2003. Image denoising using wavelet thresholding. ICGVIP, India. http://www.ee.iitb.ac.in/~icvgip/PAPERS/202.pdf

Leavline, E.J. and S. Sutha, 2011. Gaussian noise removal in gray scale images using fast multiscale directional filter banks. Proceedings of the IEEE International Conference on Recent Trends in Information Technology, June 3-5, 2011, Chennai, Tamil Nadu, pp: 884-889.

Leavline, E.J., S. Sutha and D.A.A. Gnana, 2011. Wavelet domain shrinkage methods for noise removal in images: A compendium. Int. J. Comput. Appl., 33: 28-32.

Lee, T.S., 1996. Image representation using 2D gabor wavelets. IEEE Trans. Pattern Anal. Machine Intell., 18: 959-971.

Meyer, F.G. and R.R. Coifman, 1997. Brushlets: A tool for directional image analysis and image compression. Appl. Comput. Harmon. Anal., 4: 147-187.

Pennec, E.L. and S.G. Mallat, 2005. Sparse geometric image representations with bandelets. IEEE Trans. Image Process., 14: 423-438.

Soman, K.P. and K.I. Ramachandran, 2005. Insight Into Wavelets From Theory To Practice. 2nd Edn., PHI Learning Pvt. Ltd., New York, ISBN: 8120329023, Pages: 404.

Stroebel, L. and R.D. Zakia, 1995. The Focal Encyclopaedia of Photography. 3rd Edn. Focal Press, UK., ISBN-13: 9780240514178, Pages: 507.

Suresh, G.R., R. Sukanesh and S. Sudha, 2007. Wavelet based image denoising using adaptive subband thresholding. Int. J. Soft Comput., 2: 628-632.

Vaseghi, S.V., 2000. Advanced Digital Signal Processing and Noise Reduction. 2nd Edn., John Wiley and Sons Ltd., New York, Pages: 473.

Velisavljevic, V., B. Beferull-Lozano, M. Vetterli and P.L. Dragotti, 2006. Directionlets: Anisotropic multidirectional representation with separable filtering. IEEE Trans. Image Process., 15: 1916-1933.

Wang, H. and J. Zheng, 2013. Comparative study of tongue image denoising. J. Comput., 8: 787-794.

Zhou, Z.F. and P.L. Shui, 2007. Contourlet-based image denoising algorithm using directional windows. Electron. Lett., 43: 92-93.